Journal of Applied Polymer Science

Effects of the Hydrophobization on Chitosan–Insulin Nanoparticles Obtained by an Alkylation Reaction on Chitosan

Emmanuel Robles,[1] Eva Villar,[2] Manuel Alatorre-Meda,[2] María. G. Burboa,[3] Miguel A. Valdez,[4] Pablo Taboada,[2] Víctor Mosquera[2]

[1]Departamento de Investigación en Polímeros y Materiales, Universidad de Sonora, Rosales y Transversal, 83000 Hermosillo, Sonora, México

[2]Laboratorio de Física de Coloides y Polímeros, Grupo de Sistemas Complejos, Departamento de Física de la Materia Condensada, Facultad de Física, Universidad de Santiago de Compostela, 15782 Santiago de Compostela, Spain

[3]Departamento de Investigaciones Científicas y Tecnológicas, Universidad de Sonora, Rosales y Transversal, 83000 Hermosillo, Sonora, México

[4]Departamento de Física, Universidad de Sonora, Rosales y Transversal, 83000 Hermosillo, Sonora, México

Correspondence to: M. A. Valdez (E-mail: mvaldez@correo.fisica.uson.mx)

ABSTRACT: In this work, we investigate the influence of chitosan hydrophobization on the formation, physicochemical properties, solubilization, and release profiles of chitosan-based nanoparticles (NPs) complexed with the protein insulin, used as a protein model. We use an alkylation procedure to insert 8, 10, and 12 carbon chains along the chitosan macromolecule with a final 5, 10, or 50% substitution degree. Nuclear magnetic resonance (NMR) and infrared spectroscopes (IR) were used to evaluate the success and extent of the hydrophobization procedure. The size, shape, and charge of bare polymer and polymer-insulin NPs were evaluated by dynamic light scattering (DLS), transmission electron (TEM), and atomic force (AFM) microscopes, and zeta potential, respectively. DLS and zeta potential data demonstrated that polymeric NPs made with hydrophobized chitosans possess smaller sizes and higher positive charges than NPs obtained with unmodified chitosan. Also, TEM and AFM images showed that modified chitosan-made NPs have more elongated structures. Isothermal titration calorimetry (ITC) was used to determine the type and extent of the existing interactions between the different constituting components of complexed insulin-hydrophobized chitosan nanoparticles. The association efficiency and loading capacity of insulin into the polymeric nanoparticles were also investigated under different solution conditions. Our results showed that hydrophobized chitosan-based NPs possess both higher association efficiencies and protein loading capacities at pH 6 in comparison with unmodified chitosan-based ones. *In vitro* protein release studies at pH 5.3, 6, and 7.4 demonstrated that insulin is released more slowly from hydrophobized chitosan NPs, which would favor a more sustained protein release. © 2012 Wiley Periodicals, Inc. J. Appl. Polym. Sci. 129: 822–834, 2013

KEYWORDS: biopolymers and renewable polymers; proteins; drug delivery systems; nanostructured polymers; surfaces and interfaces

Received 8 August 2012; accepted 24 November 2012; published online 15 December 2012
DOI: 10.1002/app.38870

INTRODUCTION

Although their possible safety has not yet been completely proved, nanoparticles, and special polymeric NPs, have been tested as potential vehicles for drug, protein, and peptide delivery. They demonstrated to be an exciting alternative to solve some of the difficulties associated to direct drug administration by modulating their physicochemical characteristics.[1–3] For example, NP polymeric formulations have been used to increase the concentration of solubilized hydrophobic drugs in aqueous solution, which is thermodynamically limited by their aqueous solubility,[4,5] by favoring their internalization in the hydrophobic core of the NPs, hence, allowing the increase of their bioavailability[5] and prolonging their circulation time. Their submicron size and large specific surface area also favor their absorption compared with larger particles.[6] Also, NPs can provide a greater stability and protection of the cargo in biologic fluids, a more suitable biodistribution, a sustained release pattern, and a reduction in systemic side effects.[7]

In recent years, a number of potential oral insulin-loaded polymeric nanoparticles have been developed.[8–10] However, most of

Additional Supporting Information may be found in the online version of this article.

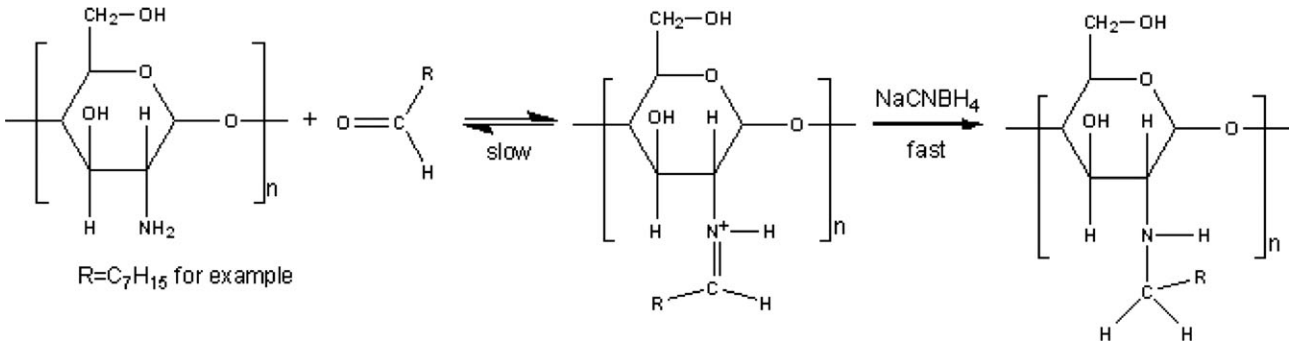

Figure 1. Diagram of the alkylation reaction on chitosan.

these systems still present different concerns such as their stability in GI tract, a low intestinal epithelium absorption, a low insulin loading efficiency, or the existence of burst release phases. For this reason, different researchers have explored the nasal and pulmonary surfaces as an alternative to the oral route for insulin administration to increase protein adsorption at the nasal or pulmonary mucosa to achieve optimal insulin concentrations.[11–13] To achieve this goal, the biopolymer chitosan and their formulating NPs appear as excellent candidates. Chitosan is a cationic polysaccharide obtained by partial deacetylation of chitin, the major component of crustacean shells.[14] It is a hydrophilic cationic polymer with outstanding properties such as biocompatibility, biodegradability and, of vital importance, mucoadhesivity.[14,15] It is also biologically inert, safe for human use, and stable in natural environments.[16] Therefore, the above characteristics make chitosan suitable for its use in a number of biomedical applications, including artificial skin, tissue regeneration, and, of course, in drug/gene delivery.[17–22] To regulate and improve the solubilization and release kinetics of different cargo molecules, hydrophobic modifications of the chitosan backbone have been performed by, for example, grafting deoxycholic,[23,24] linolenic,[25] and deoxycholic acids,[26] respectively. In particular, Zhang et al.[27] found that for oleoyl chitosans longer hydrophobic chains and larger hydrophobic groups help stabilize the NP's structure and protect the chemotherapeutic drug doxorubicin. They observed that at pH 7.4 a sustained release after a previous burst phase took place, whereas, the drug was rapidly and completely released from the NPs at pH 3.8. Recently, Sonia et al.[28] found that despite possessing excellent muchoadhesive properties, *in vitro* release profile experiments of insulin-oleoyl chitosan NPs at pH 7.4 showed that about 90% of insulin was released in 5 h. Jo et al.[29] also obtained hydrophobic glycol-chitosan NPs with a slow insulin release profile and longer activity *in vivo* than bare chitosan NPs as a result of insulin association to the glycol chitosan nanoparticles, through combined hydrophobic and ionic interactions; however, insulin association efficiency (AE) was rather low (ca. 20 %).

In this work, we investigate the physicochemical properties of insulin–chitosan NPs based on hydrophobically derivatized chitosans to perform a future evaluation *in vivo* as potential protein delivery systems for nasal or pulmonary administration.

The main objective of the present work was to obtain a NP system capable of simultaneously modulate and control the insulin delivery at different pH in contrast to simple chitosan–insulin nanoparticles, by lowering the initial insulin burst phase while keeping the insulin delivery for longer times through increases of the hydrophobicity of the chitosan molecule. To do this, the chitosan backbone was grafted with hydrophobic chains of 8, 10, and 12 carbons by using an alkylation method.[30,31] We hypothesized that the amphiphilic protein insulin can be loaded into hydrophobized chitosan NPs by exploiting hydrophobic interactions established between the hydrophobic inner core of the chitosan NPs and the hydrophobic side chains of protein molecules. Also, electrostatic interactions between positively charged chitosan and negatively ionized insulin can contribute to the stability of the complexed protein-polymer NPs. By infrared spectroscopy (IR), nuclear magnetic resonance (NMR), and isothermal titration calorimetry (ITC), we investigated the effect of chitosan hydrophobization on the physicochemical properties of chitosan–insulin NPs. Light scattering and zeta potential experiments were performed to measure the average size and charge of the NPs, respectively, and their shape was confirmed by transmission and atomic force microscopy images. Insulin association efficiency, loading capacity, and *in vitro* release profiles were performed at different pHs for bare and hydrophobized chitosan NPs.

EXPERIMENTAL

Materials

Chitosan with an average molecular weight of 415,000 g/mol and 90% degree of deacetylation (Fluka, cat. no. 28191, middle viscosity grade) was used. Sodium cyanohydroborate ($NaCNBH_4$), octyl aldehyde, decyl aldehyde, dodecyl aldehyde, insulin (human recombinant, 1 mg equivalent to 29.1 USP units), and pentasodium tripolyphosphate (TPP) were purchased from Sigma (Sigma-Aldrich Co.; USA) and used as received. Water was filtered with an Easy pure/Barnstead instrument with a resistivity of 18.3 MΩ-cm. All organic solvents were of HPLC grade and all other chemicals were reagent grade.

Methods

Synthesis of Chitosan Derivatives. Chitosan derivatives were obtained by a reductive amination process following a procedure previously described in the literature.[31,32] This method produces a covalent bond between a substrate and the amine group of chitosan (see Figure 1). Substrates in our work were 8, 10, and 12-carbon hydrocarbon chains. The alkylation reaction was performed as follows: 2 g of chitosan were dissolved in

110 mL of acetic acid (0.2 M). After complete dissolution, 75 mL of ethanol were added to allow the aldehyde to be in a solvating medium. pH was adjusted to 5.1 to avoid the precipitation of chitosan. A corresponding aldehyde proportion (5, 10, or 50%) was diluted in ethanol and added to the chitosan solution; thereafter, an excess of sodium cyanohydroborate (3 : 1 chitosan mol basis) was added. The mixture was stirred for 24 h at room temperature, and the alkylated chitosan was precipitated with ethanol. Then, pH was adjusted to 7 and the precipitate was washed several times in ethanol/water mixtures of increasing ethanol content from 70 to 100% v/v. In this manner, we synthesized a variety of hydrophobic derivatives of chitosan by modifying the length of the hydrophobic chain (8, 10, and 12 carbon) and the substitution degree along the chitosan backbone (5, 10, and 50%). The calculated pKs of the hydrophobized chitosans were: 6.52 for 5% substituted chitosans, 6.54 for 10% substituted chitosans, and 6.8 for 50% substituted chitosans, respectively.[33]

Preparation of Chitosan Nanoparticles. Chitosan (CNPs) and chitosan–insulin NPs (CINPs) were prepared by following the methodology previously described by Fernández-Urrusuno et al.[11] and Zengshuan et al.[34] with modifications. Chitosan (1 mg/mL) was dissolved in acetic acid (6 μM) while TPP (0.5 mg/mL) was dissolved in NaOH (0.01 M). For the production of CINPs, insulin (1 mg/mL) was dissolved in HCl (0.01 M), 2 mL of the protein solution were premixed with 1 mL of TPP before dropwise addition into 4 mL chitosan solution. In the case of CNPs, TPP solution was directly dropped into the chitosan solution. Magnetic stirring was kept at 500 rpm at room temperature for 30 min. The final pH of the NP suspension was controlled by adjusting the pH of the insulin/TPP or TPP solutions prior addition, with a final value of 5.3 unless otherwise stated. The NPs characterized immediately after stirring. The pH of 5.3 was selected in the light of previous studies showing an improved insulin complexation with chitosan at this pH value.[11,34] For the *in vitro* insulin release experiments, association efficiency (AE) and loading capacity (LC) values were also obtained at pH 6 for comparison. In order to make a direct comparison of the resulting data we used the same fixed proportions of chitosan/insulin (4/2 w/w) and chitosan/TPP (4/1 w/w) in the elaboration of the NPs as reported in previous works.[11,29]

Dynamic Light Scattering. Dynamic light scattering (DLS) measurements were performed using an ALV-5000 digital correlator system (ALV 5000/E, ALV GmbH, Germany) equipped with a temperature control set at 25 C ± 0.1°C. The scattered light was vertically polarized with a $\lambda_0 = 488$ nm solid-state laser (2W). The hydrodynamic radius, R_H, was obtained for diluted samples from DLS measurements at an incidence angle of 90° by analysis of the DLS data using the CONTIN algorithm developed by Provencher and Stepanak[35] and applying the Stokes-Einstein equation, $R_H = kT/6\pi\eta D$, where k is the Boltzmann constant, T the temperature, η the solution viscosity, and D the diffusion coefficient of the particles in diluted solution. Measurements were performed in triplicate with a sampling time of 60 s each and averaged.

Transmission Electron Microscopy. To acquire transmission electron microscopy (TEM) images, a drop of CNP and CINP suspensions were applied to carbon-coated copper grids, blotted, washed, negatively stained with 2% (w/v) of phosphotungstic acid, air dried, and then examined with a Phillips CM-12 transmission electron microscope operating at an accelerating voltage of 120 kV. Samples were diluted 20- to 200-fold when necessary before deposition on the grids.

Atomic Force Microscopy. Nanoparticle morphology was observed through an AFM instrument model JSPM-4210 (JEOL, Japan). A drop of NP suspension was deposited onto freshly cleaved mica and air-dried for several minutes. Images were observed in the noncontact mode by using a NSC15 silicon cantilever (MikroMasch, Oregon, USA). Atomic force microscopy (AFM) images were analyzed with the WSxM software.[36]

Infrared Spectra (FTIR). Chitosan NPs were isolated by centrifugation at 10,000 × g for 20 min and dried. IR spectra were acquired with a FTIR instrument (Perkin-Elmer, model Spectrum GX) coupled to a PC. Samples were directly mixed with KBr pellets in the sample holder and placed in the trajectory of an IR laser beam; the transmittance was observed for the mid-IR range of 400–4000 cm^{-1}. The IR spectra were collected sixteen times (spectral resolution 4 cm^{-1}) and analyzed using Spectrum software.

Nuclear Magnetic Resonance (^{1}H-NMR). High resolution nuclear magnetic resonance (^{1}H-NMR) spectra were recorded on a Bruker (Avance, 400 MHz) spectrometer. A 5 mg of different samples were dissolved at 40°C in 0.5 mL of a 2% v/v deuterium chloride/D_2O (pH 3.2). The solutions were then freezed/defreezed three times to exchange labile protons with deuterium and their spectra were recorded at 300 K. Tetramethylsilane was used as a reference.

Zeta Potential. Zeta potential of CNP and CINP NPs was measured by using a Nano ZS (Nanoseries, Malvern Instruments, UK). The instrument measured the electrophoretic mobility of the particles and converted it to the Zeta-potential using the classical Smoluchowski expression:

$$\alpha = \varepsilon\frac{\zeta}{\eta}, \tag{1}$$

where α, ε, ζ, and η denote the electrophoretic mobility, permittivity of the media, zeta-potential of the particles, and viscosity of the media, respectively. Each sample was fed into a folded capillary, clear, disposable zeta cell. Measurements were initiated after attaining thermal equilibrium at 25°C. The number of runs in each measurement was automatically determined by the software. Results were reported as the mean ± standard deviation (SD).

Isothermal Titration Calorimetry (ITC). Binding studies were performed using a VP-ITC titration microcalorimeter from MicroCal Inc.; (Northampton, MA) with a cell volume of 1.436 mL at 25°C. Samples were degassed in a ThermoVac system (MicroCal) prior to use. The sample and reference cells were filled with the cationic chitosan solution (8×10^{-4} mM) dissolved in 10 mM acetate buffer (pH 4.8) and pure buffer solution, respectively. The anionic solution containing insulin (0.085 mM) and TPP (2.88 mM) dissolved in 0.01M NaOH at pH 9.27 was introduced into the thermostated cell by means of a syringe and stirred at 350 rpm, which ensured rapid mixing

but did not cause foaming on solutions. Each titration experiment consisted of an initial 2 μL injection (neglected in the analysis) followed by 23 subsequent 12 μL injections programmed to occur at 400 s intervals, sufficient for the heat signal to return to the baseline. We present the results of the ITC experiments in terms of the heat of injection normalized by the insulin concentration added per each injection, Q^*, as a function of the insulin/chitosan molar ratio. Heats of dilution from titrations of the anionic solution into acetate buffer only (without chitosan) were subtracted to obtain the net binding heats. All experiments were carried out in duplicate and the reproducibility was within $\pm 3\%$.

Raw data of ligand binding (insulin, in our case) to chitosan were analyzed as described previously[37,38] on the basis of the single set of identical sites model supplied by the MicroCal software (Origin v. 7.0). This model employs the following fitting equation that correlates the heat per injection, Q, with the binding stoichiometry n, the fractional sites of macromolecule occupied by ligand θ, the macromolecule concentration M, the binding enthalpy ΔH, and the cell volume V:

$$Q = n\Theta M \Delta H V \tag{2}$$

One can solve the former equation for Θ by using the equilibrium equation for the binding constant K, with X as the total concentration of ligand and [X] as the concentration of unbound ligand:

$$K_b = \frac{\Theta}{(1-\Theta)[X]}, \quad [X] = X - n\Theta M \tag{3}$$

To achieve an accurate fit of all three floating parameters to our data, multiple attempts were performed starting from different initial parameters. The same three values were reached at the minimum χ^2, regardless of the values of initialization.

Quantitative Analysis of Insulin in the NPs. To determine the association efficiency (AE) and loading capacity (LC), CINPs were pelletized at 8500 rpm (Microfuge 22R centrifuge, Beckman Coulter Inc.; USA) at room temperature for 20 min. The insulin content in the supernatant was measured by the microBCA protein assay (Sigma-Aldrich, USA). A calibration curve was made using the supernatant of each CNP system as a blank. Each sample was measured in triplicate. The AE and LC were calculated by the following expressions:

$$\mathrm{AE} = \frac{(\text{total amount of insulin} - \text{insulinin supernatant})}{(\text{total amount of insulin})} \times 100\% \tag{4a}$$

$$\mathrm{LC} = \frac{(\text{total amount of insulin} - \text{insulin in supernatant})}{(\text{weight of nanoparticles})} \times 100\% \tag{4b}$$

***In Vitro* Release Studies.** The insulin release ability from the polymeric complexed NPs were measured *in vitro* at a constant temperature of 37°C and three different pH in order to analyze the influence of this factor on the protein release profiles. CINPs were incubated at physiological pH 7.4, and at pH 6 and 5.3, which lie in the range of the nasal mucosal pH.[39] Large excesses of phosphate buffer or acetate buffers at the same pH values were used, respectively, to ensure sink conditions. The released insulin concentration was determined at different times for each evaluated pH by means of the MicroBCA protein assay (Sigma-Aldrich, USA) by using a protein calibration curve as a standard.

RESULTS AND DISCUSSION

Chitosan NPs were spontaneously formed by the previously developed ionotropic gelation technique.[11] This technique is based on the existence of electrostatic interactions between the positively charged amino groups of chitosan (polycation) and the negatively charged TPP (polyanion), resulting in a nanocarriers suitable for incorporation of different cargos, such as insulin. Reversible electrostatic crosslinking, instead of chemical cross-linking, has been applied to avoid the possible toxicity of reagents and other undesirable effects. This technique involves the mixing of two aqueous phases at room temperature with slow stirring to ensure complete formation of the NPs. Therefore, it does not employ organic solvents or sonication (although optional) common to other preparative methods which, however, may be harmful for peptides and proteins.

The properties of chitosan NPs (CNPs) and chitosan–insulin NPs (CINPs) were investigated by using an unmodified medium molecular weight chitosan, Qm, and derivatized chitosans with octyl aldehyde, labeled as Qm8a, Qm8b, and Qm8c, or dodecyl aldehyde (labeled as Qm12a, Qm12b, and Qm12c) with a 5, 10, and 50% (denoted as a, b, and c, respectively) degree of substitution on the polymer main chain. Also, in some cases CNPs and CINPs were obtained with derivatized chitosan with a degree of substitution of 10% with decyl aldehyde (Qm10b) in order to compare the effect of the hydrophobic chain length at a specific substitution degree on the size, charge, AE, LC and *in vitro* insulin release experiments.

Confirmation of the Hydrophobization Procedure

In order to check the success of the hydrophobization of the chitosan backbone and the degree of substitution, ^{1}H-NMR and FTIR experiments were performed.

^{1}H-NMR. ^{1}H-NMR spectra of bare chitosan and three hydrophobized chitosans (Qm8a, Qm8b, Qm8c) are shown in Figure 2 as an example. The peak at 5.08 ppm is assigned to water, while the peaks at 4.6 and 4.8 ppm were assigned to the H-1 protons of the glucosamine and *N*-acetyl glucosamine residues, respectively. The ring protons (H-3, 4, 5, 6, 6′) were considered to resonate at 3.7–3.9 ppm,[40] while the peak at 3.1–3.2 ppm can be ascribed to a H-2 proton of *N*-acetyl glucosamine or glucosamine residues.[41–43] Peaks at 2.0–2.1 ppm can be assigned to the three *N*-acetyl protons of *N*-acetyl glucosamine. Peaks at 0.8, 1.3, and 1.7 ppm were exclusive of the substitution reaction and ascribed, respectively, to CH_3, —CH_2—, and —CH_2—(C—N) of the octyl residue. The intensities of the latter peaks directly vary with the degree of substitution enabling its estimation and, hence, the confirmation of the target formulae. We also performed a microanalysis of the experimental data obtaining the following proportions of the hydrophobic substituent: 5.4% for

Applied Polymer SCIENCE

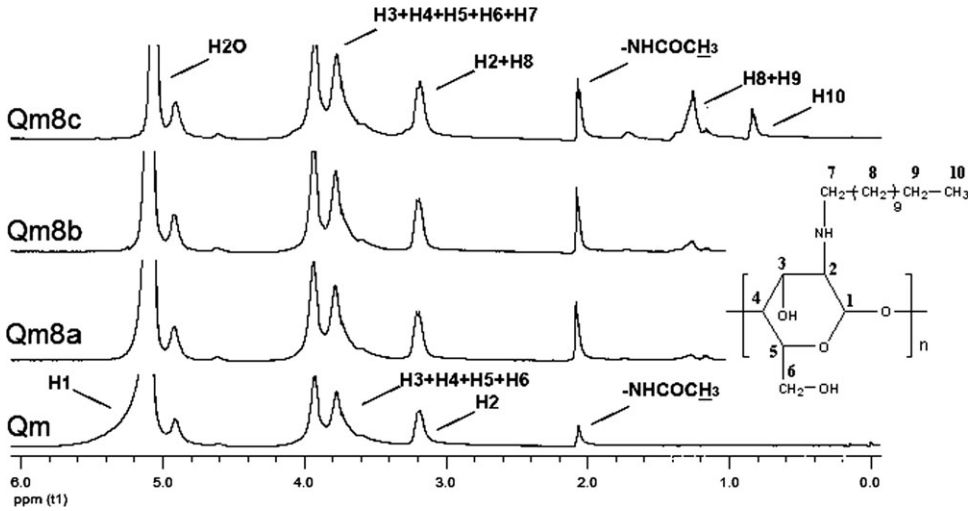

Figure 2. ^{1}H-NMR spectra of unmodified chitosan Qm and three different hydrophobic chitosans derivatized with eight carbon chains, substituted 5% (Qm8a), 10% (Qm8b) and 50% (Qm8c), respectively on the chitosan molecule.

Qm8a, 10.8% for Qm8b, and 44.14% for Qm8c, respectively.[32,44] These results confirm the completeness of the alkylation reaction.

FTIR. Further corroboration about the success of the chitosan hydrophobization process was gained through FTIR spectroscopy. FTIR spectra of unmodified and hydrophobic chitosans with a degree of substitution of 10% with 8, 10, and 12 carbon chains, and their corresponding NPs in the presence and absence of insulin are shown in Figure 3. According to FTIR, native chitosan [Figure 3(a)] shows a broad band located between 4000 and 2800 cm^{-1} associated with the stretching of —NH_2 and —OH groups.[45] We can observe two characteristic peaks at 2933 and 1883 cm^{-1} corresponding to the CH_2 stretching vibration attributed to the pyranose ring. The two peaks at 1650 and 1597 cm^{-1} are assigned to the carbonyl group and amino group of amide I band, respectively. For modified chitosans, we observed important changes in the latter band pointing that hydrogen bonding is decreasing as a result of the reaction between the aldehyde and amine groups of chitosan. Apparently, these changes are more evident when the length of the bonded aldehyde chain is increased, as observed in Figure 3(c,d). The presence of a peak at 3153 cm^{-1} and a shoulder at 1557 cm^{-1} can be assigned to secondary amines (–NH bending vibration), suggesting that the hydrophobic chain is bonded to the amine groups of chitosan. Also, the peak at 1400 cm^{-1} is assigned to the CH_2 deformation of the aliphatic chain [Figure 3(b–d)]. Finally, the bands observed for hydrophobic chitosans in Figure 3(b–d) at about 2330 and 2170 cm^{-1} correspond to cyanide ions or hydride vibrations from the borane bond (B-H)[46] originated from the residues of the chitosan hydrophobization.

The FTIR spectra of CNPs and CINPs displayed prominent changes when compared with native and hydrophobically modified chitosan backbone chains. For instance, the band located between 4000 and 2800 cm^{-1} is broader for CNPs and CINPs regarding native and hydrophobically modified chitosans, probably as a result of the addition of TPP which promotes the formation of new hydrogen bonds inNPs.[47] Also, this band is broader for CINPs than for CNPs, in agreement with the presence of insulin in the NP. The presence of TPP is revealed by both the shoulder at 2500 cm^{-1} and the peak for P = O at 1150 cm^{-1}.[48] In addition, we can observe the disappearance of the peak located at 1594 cm^{-1} and the emergence of a new one at 1556 cm^{-1} for both CNPs and CINPs. This effect can be attributed to the linkage between phosphoric and ammonium ions.[47] On the other hand, the loading of insulin into the CINPs is usually probed by means of the identification of protein typical bands as the N—H bending for amide I (1700–1600 cm^{-1}) and amide II (1580–1480 cm^{-1}). Nevertheless, there exists an overlapping of the bands corresponding to the carbonyl groups of amide from the chitosan backbone and amide I from insulin, so that the presence of insulin in the CINPs is corroborated by the band corresponding to the C-N stretching of amide III (1300–1200 cm^{-1}), which appeared at 1230 cm^{-1}.[49]

Energetics of the Formation of the Polymeric-Based NPs

The capability of any given drug delivery system to avoid premature dissociation and promote the cargo release to the target organ or tissue is strongly related to the binding affinity between the therapeutic macromolecule and the vehicle in question. One way to assess such an interaction is to measure by ITC the drug-vehicle binding heat upon complexation and from suitable modelization of this property to calculate the binding thermodynamics. In order to determine the insulin–chitosan heat of binding in the presence of TPP crosslinker, we run two different experiments. In the first experiment, we titrated the anionic solution containing insulin and TPP into the sample cell containing chitosan. In a second experiment, conducted as a blank, we titrated a TPP solution into the sample cell containing chitosan. Reported results were calculated after subtracting the blank from the first experiment. In this way, heats from insulin dilution and TPP-chitosan interactions were neglected. With these experiments we tried to evaluate how the degree of substitution can affect the energetics of the insulin–chitosan association. Figure 4 shows the insulin–chitosan heat of

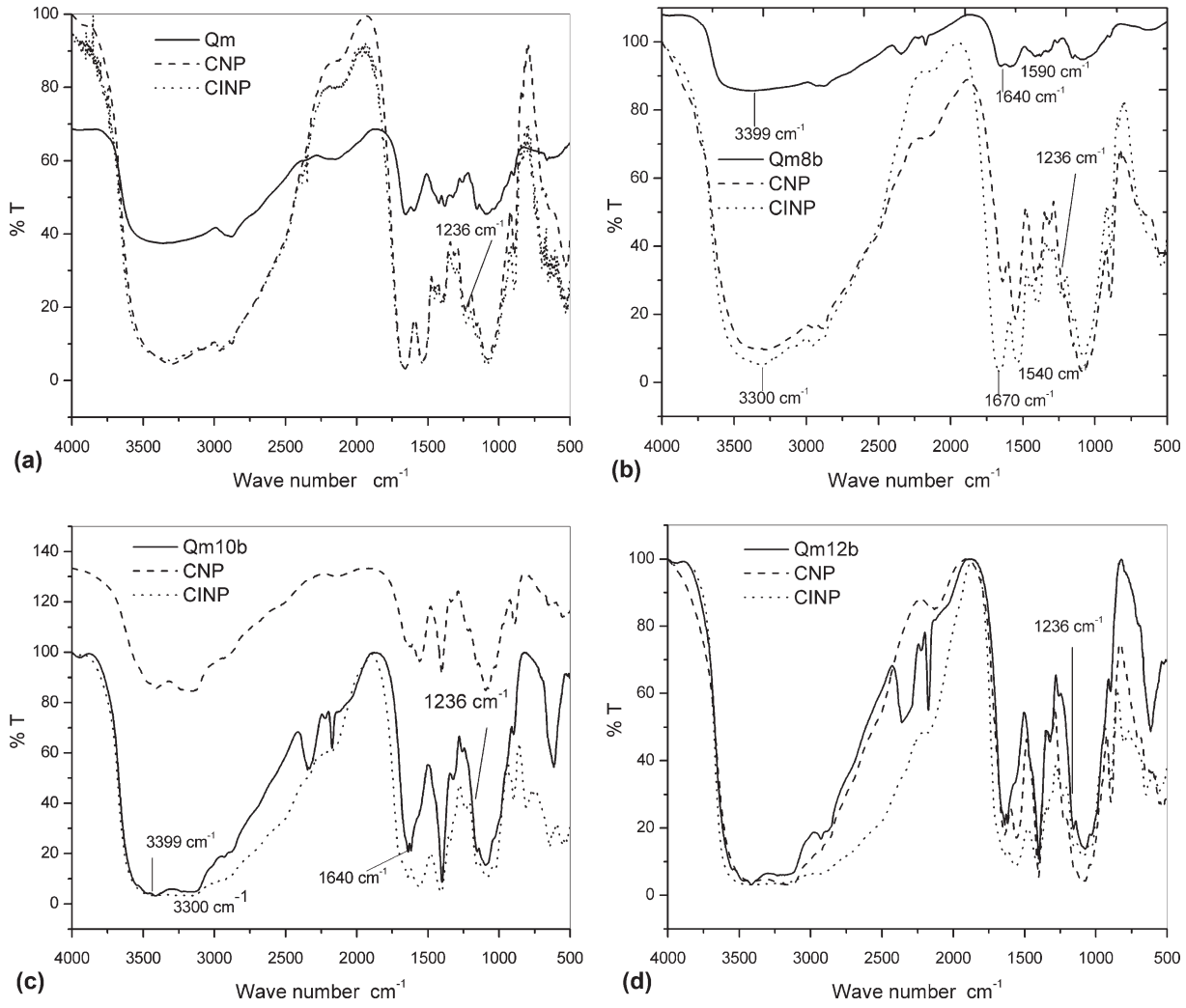

Figure 3. FTIR spectra of unmodified chitosan, 10% substituted hydrophobized chitosans and the corresponding nanoparticles with (CINP) and without (CNP) insulin. (a) native chitosan, (b) derivatized chitosan with eight carbon chains, (c) derivatized chitosan with 10 carbon chains, and (d) derivatized chitosan with 12 carbon chains.

interaction normalized by the insulin concentration added per each injection, Q^*, as a function of the insulin to chitosan molar ratio for NPs formed with unmodified and hydrophobized chitosans with different degrees of substitution (final solution pH about 5.3). Solid lines represent the fits to experimental data. It can be observed from this figure that the binding of insulin to chitosan in the presence of TPP proceeded into two well-differentiated stages in all cases. The first binding stage was recorded as a gradual increment in released heat up to a local, exothermic minimum. Meanwhile, the second binding stage occurred upon further injections of insulin (and TPP) originating a steep reduction in the released heat up to markedly lower exothermic values, not even reaching thermal equilibrium. Analyzing the whole process of the NPs formation, the local increase in released heat at early injections reveals the strong implications of electrostatics in the insulin–chitosan binding at low insulin/chitosan molar ratios where chitosan is expected to be in excess. As expected, such an effect was found to be accentuated (larger variation of released heat) upon insulin injection

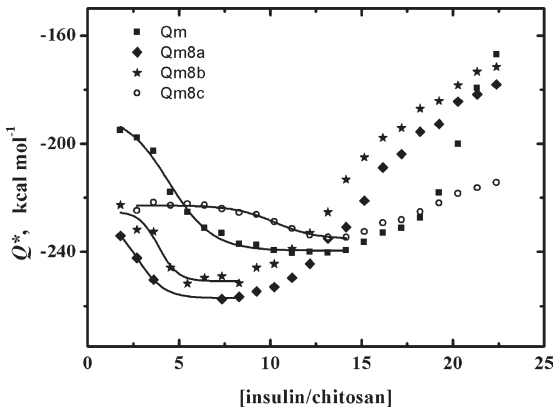

Figure 4. Integrated heat of interaction between insulin and unmodified and modified chitosans (eight carbons) upon formation of NPs as a function of the insulin to chitosan molar ratio. Solid lines represent the mathematical fitting to the experimental data. Heat contributions from dilution were subtracted. Temperature of the cell was 25°C.

Table I. Thermodynamic Parameters of Interaction Between Insulin and Chitosan Upon Formation of the Insulin–Chitosan NPs

	$K \times 10^{-4}$ (M^{-1})	n	ΔH (kcal/mol)	ΔS (kcal/mol K)
Insulin-Qm	1.96 ± 0.12	4.29 ± 0.50	−53.9 ± 0.3	−0.16
Insulin-Qm8a	1.89 ± 0.34	2.68 ± 0.21	−30.1 ± 0.5	−0.081
Insulin-Qm8b	2.71 ± 0.92	3.88 ± 0.11	−25.9 ± 0.1	−0.066
Insulin-Qm8c	3.38 ± 0.51	10.24 ± 0.42	−12.4 ± 0.1	−0.02

K, binding equilibrium constant; n, binding stoichiometry; ΔH, enthalpy changes; ΔS, entropy changes.

in the case of NPs formed with Qm, which holds a higher number of available, nonhydrophobized amine groups.

In contrast, Qm8a and Qm8b displayed larger absolute exothermic heats upon first injections of insulin than Qm. This leads us to think that the presence of low degrees of hydrophobic substituents may involve an enhanced surface exposition of charged residues to solvent favoring electrostatic interactions with protein molecules. This view is also supported by a faster polymer-protein complexation, as denoted the presence of the exothermic minima at lower insulin/chitosan molar ratios if compared with unmodified chitosan. For Qm8c, the larger degree of substitution would enable insulin to be more progressively bound (and to a lesser extent as shown below) by both electrostatic and hydrophobic interactions to the chitosan. This fact might be corroborated by the observed shift of the exothermic minimum to larger insulin–chitosan molar ratios and the decrease of the released heat values provided that hydrophobic interactions are slightly endothermic, with energies lying in the range of 0.1–0.7 kcal/mol.[50]

On the other hand, the sharp evolution of all plots to markedly lower exothermic values upon further addition of insulin (and TPP) reveals a strong structural change in the systems most likely related to the accomplishment of ionotropic gelation.[51–53] At the molecular level, complex formation between polyelectrolytes, including charged proteins and polysaccharides, can cause structural changes to either (or all) component of the complex.[53] Such structural changes, related to the condensation of aggregated complexes, produce strong, endothermic signals due to water molecules delocalization around the forming complex and the release of counterions from residual charges along the polyelectrolyte chain (charges not neutralized during the first binding stage), both occurring as the conformation of the polyelectrolyte is changing.[54,55] Consequently, the onset of the second binding stage, yielding markedly lower exothermic values, can be related to the onset of NP formation, as suggested previously.[52,56]

Thermodynamic Quantities of the Protein Complexation Process

ITC is an extremely sensitive technique in which the summation of several heat effects determines the shape of the binding isotherm. Such effects might include the dilution of both macromolecules and ligand solutions, condensation and/or aggregation of the resultant products, coupled protonation effects, and possible conformational changes upon binding.[57,58] As mentioned before, the second binding stage is expected to represent different phenomena underlying the conformational transitions occurring along the NPs formation rather than the insulin–chitosan interactions per se. Accordingly, with the aim of evaluating the insulin–chitosan interactions which definitely are believed to control the ultimate insulin release, the thermodynamic characterization was conducted by fitting only the first binding stage.[58,59] Table I summarizes the thermodynamic parameters obtained from this fitting. As observed from this table, the binding equilibrium constants obtained for all systems were found on the order of 10^4 M^{-1}, in good agreement with previously reported values for other systems including cationic polymers[58,60,61] and proteins,[62,63] and in general increasing as the substitution degree does.

The decreasing negative values of the enthalpy of interaction for Qm8a and Qm8b together with their lower stoichiometry if compared with Qm supports the notion that a lower amount of protein is interacting through electrostatic/hydrogen bonding interactions with the polymer. For Qm8c, the combination of the lowest enthalpy value and the largest stoichiometry further corroborates the idea that insulin interacts via a combination of electrostatics and hydrophobic interactions with the polymer to form the NPs. In any case, the NP assembly is still enthalpy-driven as depicted by the negative values of the entropy change even for modified chitosan Q8mc. We will analyze in great detail the thermodynamics of the interaction and the role the hydrophobic side chain lengths play in the complexed protein–chitosan NPs in a forth coming publication.

Size, Charge, and Shape of the Polymeric NPs

Dynamic Light Scattering Experiments (DLS). CNPs and CINPs at a final solution pH of 5.3 were analyzed by DLS and the obtained results are presented in Table II. As observed from this table, CINPs showed, in general, bulkier sizes than the corresponding CNPs. We notice that CNPs and CINPs made with

Table II. Average Diameter (nm) Measured by DLS and Zeta Potential (mv) of Chitosan Nanoparticles (CNP) and Chitosan–Insulin Nanoparticles (CINP) for the Nanoparticles Preparation at pH 5.3 and Room Temperature

Chitosan	CNP (nm) Average diameter	CINP (nm) Average diameter	CNP (mv) Zeta potential	CINP (mv) Zeta potential
Qm	360 ± 60	500 ± 70	8 ± 3	7 ± 3
Qm8a	260 ± 15	280 ± 20	18 ± 3	20 ± 4
Qm8b	120 ± 40	430 ± 30	27 ± 4	32 ± 4
Qm8c	140 ± 26	236 ± 40	19 ± 3	28 ± 4
Qm12a	310 ± 20	360 ± 30	24 ± 3	31 ± 4
Qm12b	300 ± 35	400 ± 50	28 ± 4	27 ± 4
Qm12c	250 ± 30	300 ± 35	22 ± 4	29 ± 4
Qm10b	200 ± 30	240 ± 30	24 ± 4	32 ± 4

hydrophobic chitosans were smaller than nonhydrophobized chitosan-made NPs, independently of the length and degree of substitution in the polymer backbone. This fact demonstrates the influence of side hydrophobic chains on the NP size. We also observe in Table II that the average size of CNPs increases as the hydrocarbon side chain length does at the same substitution degree, which corroborates the interaction of chitosan with the hydrophobic chains as demonstrated by NMR spectra. In addition, we also observed, in general, smaller NP sizes (within the uncertainties) as the degree of substitution degrees increases in the absence of protein. This effect might be a consequence of the compactation of the NP core to avoid the exposition of the hydrophobic side chains to solvent. In contrast, an increase in size for CINPs compared with CNPs is observed. In this case, the incorporation of the protein to the NP and a possible lower effective cross-linking by competition of TPP and insulin for chitosan may lead to an expansion of the CNIPs.

Particle size is one of the most significant determinant in mucosa and epithelial tissue uptake of NPs and in their intracellular trafficking.[64] This size modulation to smaller NPs with hydrophobized-chitosans can be advantageous: for example, small sized nanoparticles (ca. 100–200 nm) demonstrated more than threefold greater arterial uptake compared with large NPs (ca. 1 μm) since the former were able to penetrate throughout the sub-mucosal layers while the larger ones were predominantly localized in the epithelial lining.[65] Also, we checked that the initial pH conditions of chitosan and TPP/insulin solutions have a strong influence on the NP average size (see Supporting Information for details).

Zeta Potential Measurements. Zeta potential of the CNPs and CINPs are shown in Table II. Significant differences due to the hydrophobization of the chitosan backbone are observed. In all cases, the zeta potential of CNPs and CINPs was relatively high and positive, in agreement with an observed good NPs stability.[66] The positive charge of the particle surface is crucial for the interaction with the negatively charged mucosa, increasing the residence time of the nanocarriers at the absorption sites. Zeta potential of NPs formed with derivatized chitosans was higher in comparison with that of unmodified chitosan NPs. In line with their hydrophobic character, noncharged, hydrophobized chitosan side chains would be preferably arranged along the interior of the CINPs, leading to a larger exposure of positively amine charged groups, which might explain their apparently unexpected larger zeta potential values. The inclusion of insulin on the zeta potential of the CINPs for all hydrophobized chitosans was also found to produce a very slight increase in the zeta potential values if compared with the corresponding CNPs. This behavior is also unexpected since protein entrapment in and/or adsorption onto the NP surfaces would have significantly reduced the positive charges of cationic chitosan chains. However, as depicted by our ITC data (vide infra) and inferred by others as well,[34] hydrophobic interactions inside NPs are expected to play an important role in the complexation process. In fact, the observed slight increase in zeta potential might be accounted for the very small positive extra charge provided by the complexed protein molecules upon NP formation at pH 5.3 and/or a nonuniform and less extended conformation of the protein with long chain chitosan molecules, as observed in previous works[67] Carboxyl groups on the protein surface might form hydrogen bonds with amine groups at certain sites of the chitosan chain, but still maintaining a compact 3-D structure without spreading at the solution pH (5.3); then, an inner hydrophobic core (additionally assisted by the hydrophobic side chains in the derivatized chitosan molecules) would be maintained, hence, allowing a very high proportion of free amine groups. The largest zeta potential values observed for NPs with the largest loading capacities (see below) seem to support this hypothesis. Also, it is worth mentioning that NPs with a substitution degree of 10% display the highest zeta potentials values in agreement with their larger association efficiencies and loading capacities, therefore, being the most optimal for enhancing protein complexation at the conditions chosen for NP formation. By contrast, unmodified chitosan, Qm, gives rise to lower NP surface charges (if compared with hydrophobized chitosans) similar to those found previously by López-León et al.[68] Nevertheless, in contrast to our observations these authors showed that the addition of insulin produces CINPs with a lower positive charge, which means that the interaction would be essentially electrostatic.[69,70]

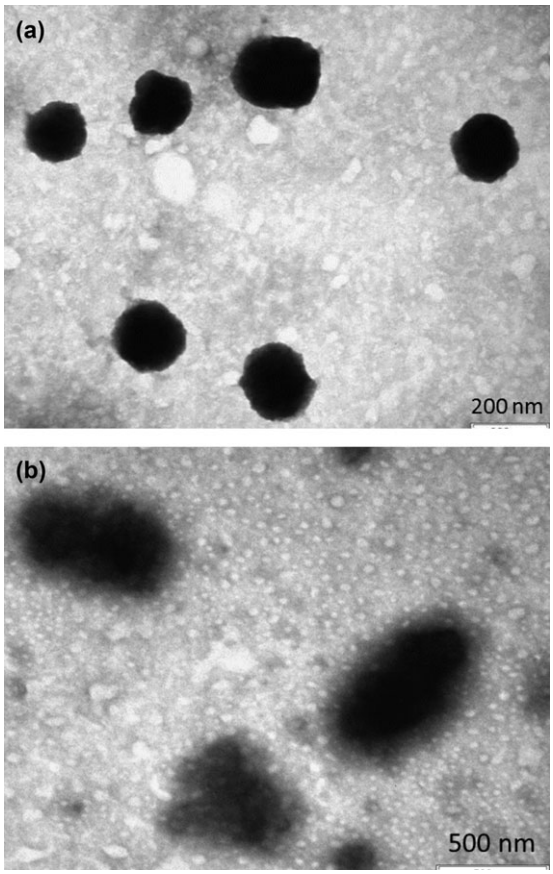

Figure 5. TEM images of CINPs obtained from (a) Qm8a and (b) Qm12b quitosans.

TEM and AFM Images of NPs. TEM and AFM images of CNPs and CINPs were obtained for the different types of chitosans. The average size of the observed NPs was in good agreement with the sizes obtained previously by DLS. The obtained images showed that the shape of the NPs seems to be dependent on the chitosans hydrophobicity to certain extent. In this regard, NPs made with unmodified chitosan or modified chitosans with the lowest substitution degree resulted in NPs with more spherical shapes [Figure 5(a)] than those formed from more

Applied Polymer SCIENCE

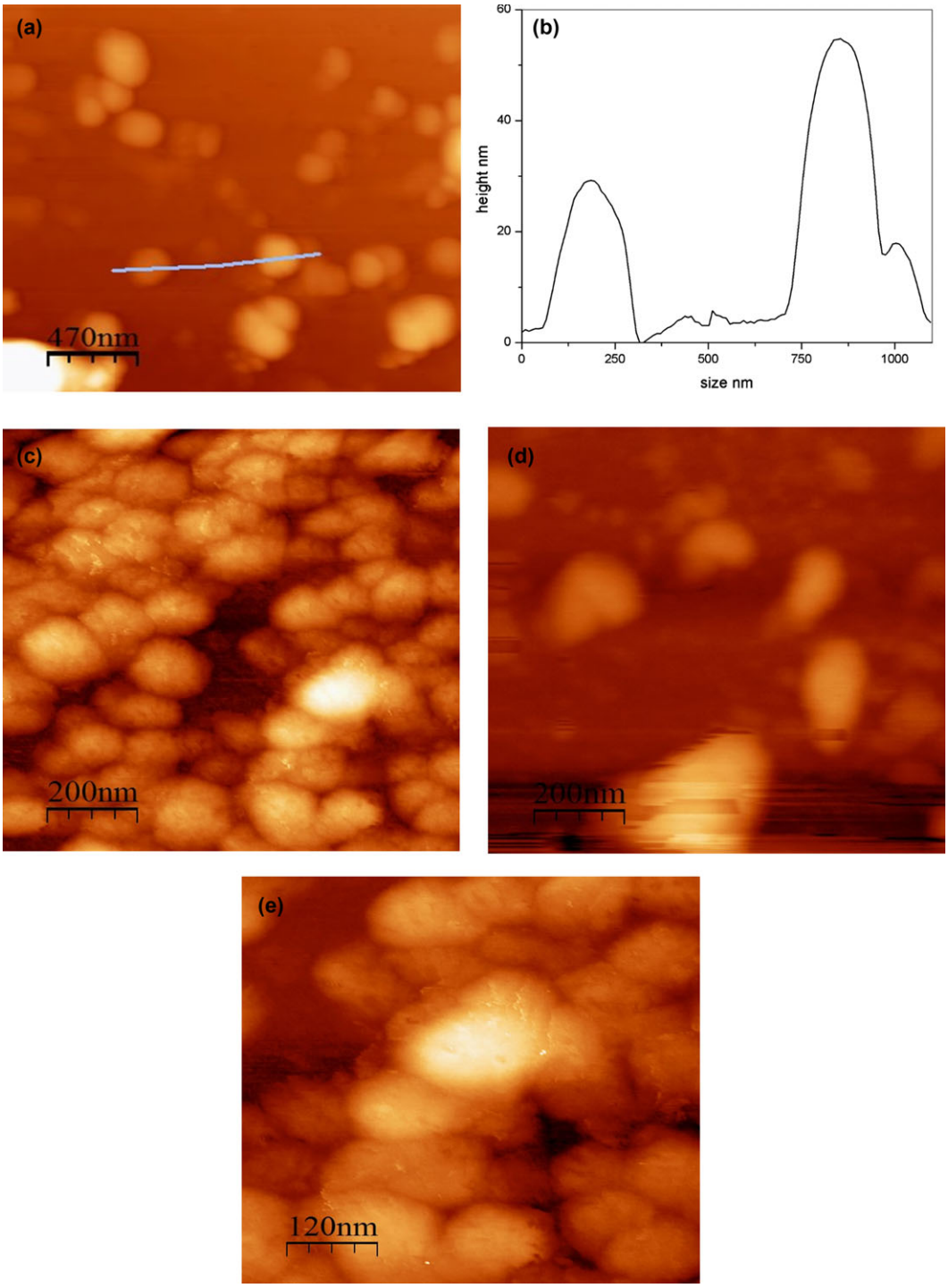

Figure 6. AFM images of CNP and CINP. (a) CNP made with native chitosan Qm, (b) height profile of two CNP seen in Figure a. (c) CNP made with Qm8b, (d) CNP made with Qm12b, (e) corresponding NP made with Qm12b including insulin. [Color figure can be viewed in the online issue, which is available at wileyonlinelibrary.com.]

hydrophobically modified chitosans used, which posses more elongated shapes as, for example, Qm12b [Figure 5(b)].

AFM images of NPs also confirmed TEM observations. CNPs made with unmodified chitosan showed spherical shapes, in agreement with TEM images [Figure 6(a)].

In Figure 6(b) the size and height profile of two NPs of Qm obtained from Figure 6(a) are shown. It is worth noting that the NP height is small in comparison with the corresponding NP diameter, which might indicate that the NPs are somehow compressed and adhered to the mica substrate through

Table III. Association Efficiency and Load Capacity of Insulin

Chitosan	AE % (pH 5.3)	AE % (pH 6)	LC % (pH 5.3)	LC % (pH 6)
Qm	63 ± 5	46 ± 4	27 ± 6	18 ± 4
Qm8a	56 ± 5	83 ± 3	18 ± 5	35 ± 5
Qm8b	60 ± 4	94 ± 5	27 ± 5	36 ± 3
Qm8c	42 ± 5	96 ± 3	17 ± 6	37 ± 5
Qm10b	30 ± 5	77 ± 5	13 ± 4	25 ± 2
Qm12a	25 ± 4	70 ± 5	11 ± 5	36 ± 4
Qm12b	55 ± 6	84 ± 5	25 ± 5	38 ± 3
Qm12c	20 ± 5	75 ± 5	22 ± 5	38 ± 3

Results of AE and LC of different chitosan–insulin nanoparticles obtained at two different pH at room temperature.

electrostatic interactions. In Figure 6(c,d), we observe that CNPs obtained from chitosans Qm8b and Qm12b show slightly elongated shapes, as previously observed by TEM. Finally, when insulin is complexed to the NPs these display a more elongated, hairy-like appearance [Figure 6(e)], which would corroborate the observed size increment detected by DLS and TEM data.

Association Efficiency, Loading Capacity, and Insulin Release from NP

Association Efficiency and Loading Capacity. To check which are the best conditions to obtain the highest AE and LC of the protein into the NPs, we screened different methodology/conditions to obtain protein-loaded chitosan/TPP NPs. Also, the effect of the solution pH where NPs were suspended on both AE and LC was analyzed provided that there exists a recognized influence of environmental pH in the crosslinking process during the formation of chitosan-TPP NPs and on their physicochemical properties.[71] In particular, we observed that lower AE values were obtained when strong acidic chitosan solutions and/or strong alkaline insulin-TPP solutions were used to produce the NPs (see Supporting Information for complete details). In the light of these results, we decide to adopt the methodology described in the Experimental section, which displayed the best results for AE and LC. Table III shows AE and LC data for CINPs obtained at final solution pH 5.3 and 6 for unmodified and different derivatized chitosans. It is firstly possible to note that both the AEs and LCs are higher at pH 5.3 than at pH 6 for unmodified chitosan as a consequence of the proximity of the chitosan pK_a to the latter pH, hence, decreasing the effective electrostatic interactions between the protein and the polymer chains. On the other hand, a better insulin association with hydrophobized chitosan NPs was observed at a final solution pH of 6, in agreement with previous reports.[34] The obtained AE and LC values at this pH are rather larger than those previously obtained for similar chitosan-based NP systems.[29,67,72,73] At pH 6, the protein can be adsorbed very efficiently onto the hydrophobically modified chitosans at a pH near the insulin isoelectric point (pI)[74] because of the minimization of electrostatic repulsion between polymer chains (which favor their aggregation and, hence, cargo entrapment) and the enhancement of hydrophobic and hydrogen interactions between polymer and protein due to the presence of the lateral hydrocarbon side chains and the decrease in the chitosan backbone net charge. In this regard, it has to be noted that insulin has an pI of 5.3 in the denatured state, but in native conditions insulin can exhibit an apparent pI of 6.4 presumably due to a masked carboxylate ionization.[75] A maximum in both AE and LC values is observed for chitosans with a degree of substitution of 10%. On the other hand, those with the largest substitution degree (50%, Qm8c and Qm12c) showed the lowest AE at pH 5.3, in agreement with the possibility of a competition effect between hydrophobic side chain compactation in the NP core and protein complexation[69,70]; by contrast at pH 6 these showed the largest AE and LC values, which additionally corroborates the influence of hydrophobic interactions in the protein loading process.

Insulin Release from Nanoparticles. Protein release from chitosan-based NPs systems is characterized by an initial fast release (burst phase) where about 30–70% of the protein diffuses to the aqueous surrounding medium within the first 3–6 h, followed by an additional slower and reduced release phase lasting for a few days. In many different treatments as for diabetes, a sustained release pattern is desired in order to maintain a constant concentration of the protein in blood and to prevent a premature leakage of the active cargo, which can lead to undesired side-effects. Hence, we analyze the insulin release profiles of our chitosan-based NPs at short incubation times to test if the hydrocarbon chains grafted on the chitosan backbones may suppress or, at least, partially mitigate the burst phase. The *in vitro* release behavior of insulin was observed to be dependent on the hydrophobicity of chitosan biopolymer and the pH of the release medium.[20] In Figure 7(a–c), we show the behavior of the insulin release at 37°C at pHs 5.3, 6, and 7.4 from CINPs made with the different types of chitosans. Briefly, it is necessary to remind that proteins encapsulated in biodegradable polymeric matrices/NPs are released by three mechanisms taking place in sequence: (i) protein desorption from the particles surface; (ii) diffusion and readsorption of the protein through the pores of the polymer network; (iii) degradation and erosion of the polymeric network. Also, solution pH affected the zeta potential values of the polymeric NPs, with approximate mean decreases of about 14 and 26 mV at pH 6 and 7.4, respectively, whereas no important changes were detected regarding NP sizes (data not shown).

First, we note that during the first hour of incubation at pH 5.3 and 7.4, insulin is more rapidly released for all CINPs, particularly, for NPs made with unmodified chitosan (more than 50% of total insulin released). After this time, a slower release profile is observed for all samples. In particular, after the first hour of incubation a linear-like release process is observed for all chitosans at pH 5.3 and 7.4, as previously observed for hydrophobic glycol chitosan NPs.[29] After 6 h of incubation at pH 5.3, 90% of insulin is released from CINPs made with Qm, while about 50% is released from the hydrophobically modified chitosan NPs except for Qm8a, which reaches a value of ca. 70%. These data are in agreement with previous results obtained in related studies using NPs made by unmodified chitosans or other hydrophobic derivatizations of this biopolymer.[29] By contrast, at pH 6 insulin is more slowly released as a consequence of the lower solubility of the chitosan chains (due to the proximity of

Applied Polymer SCIENCE

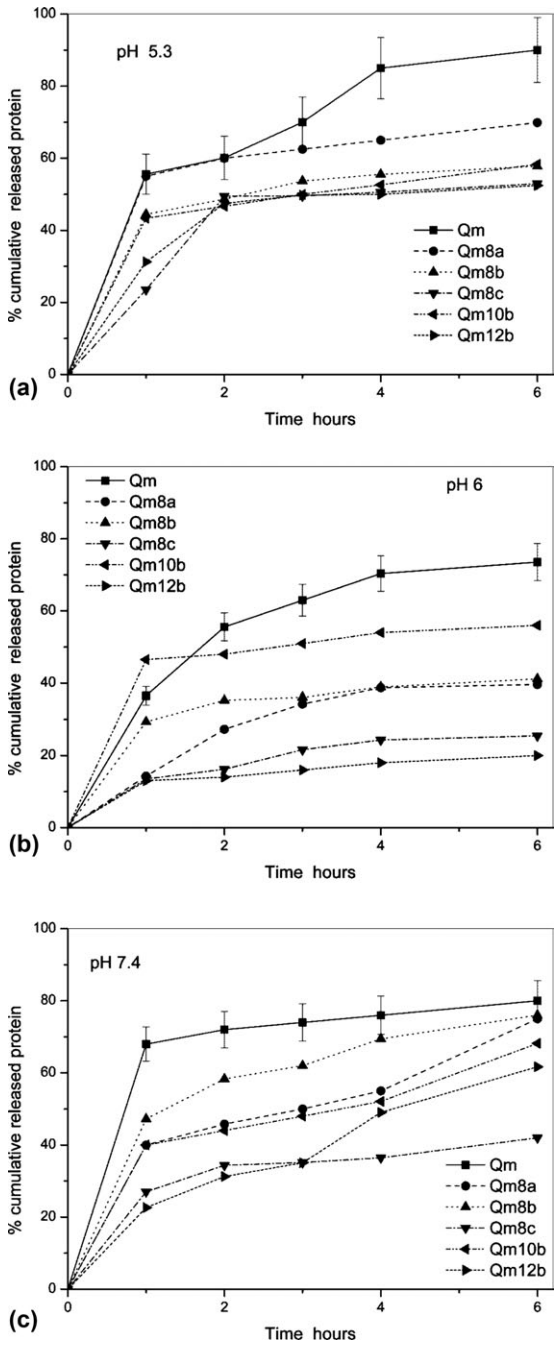

Figure 7. *In Vitro* insulin release profiles of some chitosan–insulin nanoparticles at 37°C. (a) pH 5.3 in acetate buffer, (b) pH 6 in phosphate buffer, and (c) pH 7.4 in phosphate buffer.

its pK_a), which may lead to insulin to be more tightly bounded in the NP interior instead of on the NP surface (which would lead to faster release rates), as previously noted.[11,20] In this regard, at pH 5.3 electrostatic repulsions between protein/polymer and polymer/polymer can facilitate the protein release; meanwhile, at pH 6 the release is retarded by (i) a change in the net charge of the protein (to negative) which can favor an enhancement of the interactions between carboxyl groups of the protein with the remaining protonated amino chitosan groups; (ii) an enhancement of hydrophobic interactions between chitosan chains and of chitosan/protein hydrogen bonding, especially in those NPs made with more hydrophobic polymers we used (Qm8c and Qm12b),[34] which displayed the lowest cumulative releases. The latter interactions may also play an important role on the release profile at pH 7.4. Hence, our results show that the presence of hydrophobic derivatizations in CINPs could be important to control insulin release both in *in vitro* and *in vivo* studies. Finally, it is important to mention that the structure of the protein remained unaltered upon complexation with the polymer and subsequent release, as noted from circular dichroism data (not shown).

CONCLUSIONS

In this work, we have investigated the influence of chitosan backbone hydrophobization on the formation and physicochemical properties of chitosan–insulin NPs. By an alkylation procedure, we conjugated 8, 10, and 12 carbon chains on the chitosan biopolymer with 5, 10, or 50% substitution degrees. The effect of the hydrophobization on the formed NPs was a significantly reduction of their average size both in the absence and presence of the protein. Also, TEM and AFM images showed the existence of more elongated NPs when insulin is present in the formulation. A charge increase was observed by zeta potential measurements for CINPs made by modified chitosans in comparison with CINPs made with unmodified chitosan. This arises from a larger protein loading capacity of the hydrophobically modified CINPS favored by an enhancement of hydrophobic interactions between the insulin molecules and the side chains of the chitosan molecules, probably forming the NP core. In this manner, the insulin electric charge would be conserved, and the observed zeta potential increase might be explained from the loaded protein in the NP. On the other hand, ITC experiments were performed to get further knowledge about the process of NP formation. There exists a predominant role of exothermic electrostatic interactions in this process; nevertheless, the increasing presence of the hydrophobic substitutions involves an enhancement of hydrophobic interactions which possess an endothermic character. This behavior would explain the reduction of the insulin release rate from the NPs made with hydrophobically substituted chitosans. Also, different conditions to produce CINPs at several solution pH lead to different solution behaviors and properties of the NPs. In particular, mild pHs of the chitosan, insulin and TPP solutions to produce the NPs enhanced the insulin AEs. Also, enhanced AEs and LCs were obtained for hydrophobic chitosan NPs at pH 6, in contrast to unmodified chitosan NPs.

ACKNOWLEDGMENTS

M.A. Valdez thanks the financial support of CONACyT (México) for the sabbatical leave at the Universidad de Santiago de Compostela, Spain and project # 151794; also the facilities of the Facultad de Física of Universidad de Santiago de Compostela to perform this work are acknowledged. E. Robles acknowledges CONACyT for the doctoral scholarship; P.T.A. thanks Ministerio de Economía y Competitividad for research project MAT 2010-17336, Xunta de Galicia for research projects INCITE09206020PR and 2010/50 with European Regional Development Funds, and Fundación Ramón Areces for additional financial support.

REFERENCES

1. Li, Y.; Pei, Y.; Zhang, X.; Gu, Z.; Zhou, Z.; Yuan, W.; Zhou, J.; Zhu, J.; Gao, X. *J. Controlled Release* **2001**, *71*, 203.
2. Sarmento, B.; Ferreira, D. C.; Jorgensen, L.; Weert, M. V. D. *Eur. J. Pharm. Biopharm.* **2007**, *65*, 10.
3. Chen, F.; Zhang, Z. R.; Huang, Y. *Int. J. Pharm.* **2007**, *336*, 166.
4. Soppimath, K. S.; Aminabhavi, T. M.; Kulkarni, A. R.; Rudzinski, W. E. *J. Controlled Release* **2001**, *70*, 1.
5. Gupta, V. K.; Karar, P. K.; Ramesh, S.; Misra, S. P.; Gupta, A. *Int. J. Res. Pharm. Sci.* **2010**, *1*, 163.
6. Kesisoglou, F.; Panmai, S.; Wu, Y. *Adv. Drug Deliv. Rev.* **2007**, *59*, 631.
7. Pison, U.; Welte, T.; Giersig, M.; Groneberg, D. A.; Pison, U. W. T.; Giersig, M.; Groneberg, D. A. *Eur. J. Pharmacol.* **2006**, *533*, 341.
8. Damge, C.; Reis, C. P.; Maincent, P. *Expert Opin. Drug Deliv.* **2008**, *5*, 45.
9. Damge, C.; Socha, M.; Ulbrich, N.; Maincent, P. *J. Pharm. Sci.* **2010**, *99*, 879.
10. Wu, Z. M.; Zhou, L.; Guo, X. D.; Jiang, W.; Ling, L.; Qian, Y.; Luo, K. Q.; Zhang, L. *J. Int. J. Pharm.* **2012**, *425*, 1.
11. Fernández-Urrusuno, R.; Calvo, P.; Lopez, C. R.; Jato, J. L. V.; Alonso, M. J. *Pharm. Res.* **1999**, *16*, 1576.
12. Grenha, A.; Seijo, B.; Remuñan, C. *Eur. J. Pharm. Sci.* **2005**, *25*, 427.
13. Huang, X.; Du, Y. Z.; Yuan, H.; Hu, F. Q. *Carbohydr. Polym.* **2009**, *76*, 368.
14. Berscht, P. C.; Nies, B.; Liebendörfer, A.; Kreuter, J. *Biomaterials* **1994**, *15*, 593.
15. Roberts, G. A. Chitin Chemistry; Mac Milan Press Ltd.: London, **1992**.
16. Kubota, B.; Kikuchi, Y. Polysaccharides: Structural Diversity and Functional Versatility; Marcel Dekker: New York, **1998**.
17. Dodane, V.; Vilivalam, V. *Pharm. Sci. Technol. Today* **1998**, *1*, 246.
18. Felt, O.; Buri, P.; Gurny, R. *Drug Dev. Ind. Pharm.* **1998**, *24*, 979.
19. Yao, K. D.; Peng, T.; Yin, Y. J.; Xu, M. X. *JMS-Rev. Macromol. Chem. Phys.* **1995**, *35*, 155.
20. Janes, K. A.; Calvo, P.; Alonso, M. J. *Adv. Drug Deliv. Rev.* **2001**, *47*, 83.
21. Wong, T. W. *Recent Pat. Drug Deliv. Form.* **2009**, *3*, 8.
22. Duceppe, N.; Tabrizian, M. *Biomaterials* **2009**, *30*, 2625.
23. Kim, K.; Kwon, S.; Park, J. H.; Chung, H.; Jeong, S. Y.; Kwon, I. C.; Kim, I. S. *Biomacromolecules* **2005**, *6*, 1154.
24. Lee, K. Y.; Kim, J. H.; Kwon, I. C.; Jeong, S. Y. *Colloid Polym. Sci.* **2000**, *278*, 1216.
25. Liu, C. G.; Desai, K. G. H.; Chen, X. G.; Park, H. J. *J. Agric. Food Chem.* **2005**, *53*, 437.
26. Chen, X. G.; Lee, C. M.; Park, H. J. *J. Agric. Food Chem.* **2003**, *51*, 3135.
27. Zhang, J.; Chen, X. G.; Li, Y.; Liu, C. S. *Nanomed. Nanotechnol. Biol. Med.* **2007**, *3*, 258.
28. Sonia, T. A.; Rekha, M. R.; Sharma, C. P. *J. Appl. Polym. Sci.* **2011**, *119*, 2902.
29. Jo, H. G.; Min, K. H.; Nam, T. H.; Na, S. J.; Park, J. H.; Jeong, S. Y. *Arch. Pharm. Res.* **2008**, *31*, 918.
30. Parra, H.; Burboa, M. G.; Sanchez, M.; Juarez, J.; Goycolea, F. M.; Valdez, M. A. *Biomacromolecules* **2005**, *6*, 2416.
31. Yalpani, M.; Hall, L. D. *Macromolecules* **1984**, *17*, 272.
32. Desbrières, J.; Martinez, C.; Rinaudo, M. *Int. J. Biol. Macromol.* **1996**, *19*, 21.
33. Rinaudo, M.; Pavlov, G.; Desbriéres, J. *Polymer* **1999**, *40*, 7029.
34. Zengshuan, M.; Hock-Hin, Y.; Lee-Yong, L. *J. Pharm. Sci.* **2002**, *91*, 1396.
35. Provencher, S. W.; Stepanek, P. *Part. Syst. Charact.* **1996**, *13*, 291.
36. Horcas, I.; Fernandez, R.; Gomez-Rodriguez, J. M.; Colchero, J.; Gomez-Herrero, J.; Baro, A. M. *Rev. Sci. Instrum.* **2007**, *78*, 013705.
37. Alatorre, M.; Taboada, P.; Krajewska, B.; Willemeit, M.; Deml, A.; Klösel, R.; Rodríguez, J. R. *J. Phys. Chem. B* **2010**, *114*, 9356.
38. Alatorre, M.; Taboada, P.; Hartl, F.; Wagner, T.; Freis, M.; Rodríguez, J. R. *Colloids Surf. B* **2011**, *82*, 54.
39. England, R.; Homer, J.; Knight, L.; Ell, S. *Clin. Otolaryngol. Allied. Sci.* **1999**, *24*, 67.
40. Tien, C. L.; Lacroix, M.; Ispas-Szabo, P.; Mateescu, M. A. *J Controlled Release* **2003**, *93*, 1.
41. Xu, J.; Kaplan, D. L.; McCarthy, S. P.; Gross, R. A. *Macromolecules* **1996**, *29*, 3436.
42. Signini, R.; Campana-Filho, S. P. *Polym. Bull.* **1999**, *42*, 159.
43. Sashiwa, H.; Kawasaki, N.; Nakayama, A.; Muraki, E.; Yamamoto, N.; Aiba, S. I. *Biomacromolecules* **2002**, *3*, 1126.
44. Korir, A. K., Development and Application of Microanalysis NMR Methods; University of Kansas, **2007**.
45. Yu, J. H.; Du, Y. M.; Zheng, H. *J. Wuhan Univ. (Nal. Sci. Ed.)* **1999**, *45*, 440.
46. Coates, J. Interpretation of Infrared Spectra, A Practical Approach; John Wiley & Sons Ltd.: Chichester, **2000**.
47. Bhumkar, D. R.; Pokharkar, V. B. *AAPS Pharm. Sci. Tech.* **2006**, *7*, 1.
48. Xu, Y.; Du, Y. *Int. J. Pharm.* **2003**, *250*, 215.
49. Dwivedi, N.; Arunagirinathan, M. A.; Sharma, S.; Bellare, J. *J. Nanomat.* **2010**, *2010*, 8.
50. Barbosa, S.; Taboada, P.; Mosquera, V. *Chem. Phys.* **2005**, *310*, 51.
51. Matulis, D.; Rouzina, I.; Bloomfield, V. A. *J. Mol. Biol.* **2000**, *296*, 1053.
52. Kim, W.; Yamasaki, Y.; Kataoka, K. *J. Phys. Chem. B* **2006**, *110*, 10919.
53. Turgeon, S.; Schmitt, C.; Sanchez, C. *Curr. Opin. Colloid Interface Sci.* **2007**, *12*, 166.

54. Manning, G. S. *Q. Rev. Biophys.* **1978**, *11*, 179.
55. Manning, G. S.; Ray, J. *J. Biomol. Struct. Dyn* **1998**, *16*, 461.
56. Ball, V.; Winterhalter, M.; Schwinte, P.; Lavalle, P.; Voegel, J. C.; Schaaf, P. *J. Phys. Chem. B* **2002**, *106*, 2357.
57. Wiseman, T.; Williston, S.; Brandts, J. F.; Lin, L. N. *Anal. Biochem.* **1989**, *179*, 131.
58. Prevette, L. E.; Kodger, T. E.; Reineke, T. M.; Lynch, M. L. *Langmuir* **2007**, *23*, 9773.
59. Patel, M. M.; Anchordoquy, T. J. *Biophys. J.* **2005**, *88*, 2089.
60. Nisha, C. K.; Manorama, S. V.; Ganguli, M.; Maiti, S.; Kizhakkedathu, J. N. *Society* **2003**, *20*, 5434.
61. Zhou, Y. I.; Li, Y. Z. *Spectrochim. Acta Part A Mol. Biomol. Spectrosc.* **2004**, *60*, 377.
62. Engler, L. E.; Welch, K. K.; Jacobson, L. J. *J. Mol. Biol.* **1997**, *269*, 82.
63. Milev, S.; Bosshard, H. R.; Jelesarov, I. *Biochemistry* **2005**, *44*, 285.
64. Panyam, J.; Labhasetwar, V. *Adv. Drug Deliv. Rev.* **2003**, *55*, 329.
65. Desai, M. P.; Labhasetwar, V.; Amidon, G. L.; Levy, R. J. *Pharm. Res.* **1996**, *13*, 1838.
66. Puertas, A. M.; Nieves, F. J. D. L. *J. Colloid Interface Sci.* **1999**, *216*, 2221.
67. Gan, Q.; Wang, T. *Colloids Surf. B* **2007**, *59*, 24.
68. López-León, T.; Carvalho, E. L. S.; Seijo, B.; Ortega, J. L.; Bastos, D. *J. Colloid Interface Sci.* **2005**, *283*, 344–351.
69. Elsayed, A.; Al-Remawi, M.; Farouk, A.; Badwan, A. *Sudan JMS* **2010**, *5*, 99.
70. Sadeghi, A. M.; Dorkoosh, F. A.; Avadi, M. R.; Saadat, P.; Rafiee-Tehrani, M.; Junginger, H. E. *Int. J. Pharm.* **2008**, *355*, 299.
71. Ho, J. A.; Park, H. J.; Hwang, S. J. *J. Pharm. Sci.* **2002**, *249*, 165.
72. Yan, P.; Jun, Z.; Hui, Z.; Ying, L.; Hui, X.; Gang, W. *Acta Pharmacol. Sin* **2002**, *11*, 1051.
73. Al, S.; Carrión, D.; Seijo, B.; Remuñán, C. *J. Controlled Release* **2012**, *157*, 383.
74. Muzzarelli, R. A.; Barontini, G.; Rocchetti, R. *Biotechnol. Bioeng.* **1976**, *18*, 1445.
75. Kaarsholm, N. C.; Havelund, S.; Hougaard, P. *Arch. Biochem. Biophys.* **1990**, *283*, 496.